QUANTUM SENSING

Multiparameter estimation with an array of entangled atomic sensors

Yifan Li[1]†, Lex Joosten[1], Youcef Baamara[2], Paolo Colciaghi[1], Alice Sinatra[2]*, Philipp Treutlein[1]*, Tilman Zibold[1]

In quantum metrology, entangled states of many-particle systems are investigated to enhance measurement precision of the most precise clocks and field sensors. Whereas single-parameter quantum metrology is well established, joint multiparameter estimation poses conceptual challenges and has been explored only theoretically. We experimentally demonstrated multiparameter quantum metrology with an array of entangled atomic ensembles. By splitting a spin-squeezed ensemble, we created an atomic sensor array featuring intersensor entanglement that can be flexibly configured to enhance measurement precision of multiple parameters jointly. Using an optimal estimation protocol, we achieved substantial gains over the standard quantum limit in key multiparameter estimation tasks, thus grounding the concept of quantum enhancement of field sensor arrays and imaging devices.

Atomic precision sensors, such as atomic clocks (*1*), magnetometers (*2*), and inertial sensors (*3*), play an important role in science and technology. Many state-of-the-art devices are limited by the intrinsic quantum noise associated with measurements on a finite number of sensor particles, giving rise to the standard quantum limit (SQL) (*4*). Quantum metrology aims at reducing this noise by harnessing entanglement between the particles (*5*), promising substantial improvements for sensor applications in fundamental physics and technology (*6*). Quantum metrology of a single parameter, such as the frequency of an atomic transition or a single component of a magnetic field, has been demonstrated in proof-of-principle experiments (*7*–*13*) and recently also in metrology-grade setups (*14*–*16*).

Multiparameter estimation is a new frontier in quantum metrology that is receiving great interest (*17*–*23*) because of its relevance for vector field sensors (*24*, *25*), imaging devices (*22*, *26*, *27*), sensor arrays (*18*, *28*–*33*), and clock networks (*34*). Whereas, for single-parameter quantum metrology, there is a clear theoretical framework (*5*), the joint estimation of multiple parameters with quantum sensors is surprisingly complex from a conceptual point of view. For parameters encoded by noncommuting Hamiltonians, the incompatibility of optimal measurements poses a fundamental challenge (*19*, *24*, *35*, *36*, *37*). For distributed sensing with parameters encoded by commuting Hamiltonians on spatially separated sensor modes, intriguing questions arise regarding the optimal strategy and the possible enhancements provided by intersensor entanglement (*18*, *28*–*33*). Further challenges arise from constraints on sensor control and detection and the presence of (possibly correlated) technical noise (*31*, *38*). Owing to the complexity of the problem, statements about quantum gain in multiparameter estimation generally depend on the framework adopted. Although these questions have been intensely investigated theoretically, experiments are only beginning to explore this field (*39*–*42*).

[1]Department of Physics, University of Basel, Klingelbergstrasse 82, Basel, Switzerland. [2]Laboratoire Kastler Brossel, ENS-Université PSL, CNRS, Université Sorbonne et Collège de France, 24 rue Lhomond, Paris, France. ***Corresponding author. Email: alice.sinatra@lkb.ens.fr (A.S.); philipp.treutlein@unibas.ch (P. T.)** †Present address: Laboratoire Kastler Brossel, ENS-Université PSL, CNRS, Université Sorbonne et Collège de France, Paris, France.

A paradigmatic system for multiparameter quantum sensing is an array of spatially separated atomic ensembles that can be individually controlled and detected (*18*, *27*, *29*, *33*), such as in an atomic field imaging sensor (*43*, *44*) or optical lattice clock (*16*). The parameters are local spin rotation angles imprinted on the ensembles and the task is to estimate these parameters or certain nonlocal linear combinations of interest. Previous experiments demonstrated quantum gain in estimating a single parameter combination with distributed entanglement (*40*, *41*). The scenario considered in this work is a true multiparameter estimation problem, where each sensor reveals a local parameter value in each experimental run, and the question is how entanglement within each ensemble and between the ensembles can enhance measurement precision in multiple parameters jointly. This may require adapting the input state dynamically within the given set of resources (*27*). These questions have recently attracted considerable theoretical interest, and different sensing protocols have been proposed (*18*, *27*, *29*, *32*, *33*), but experimental demonstrations of multiparameter estimation with entangled atomic ensembles are lacking.

In this work, we used an array of atomic Bose-Einstein condensates (BECs) whose collective spins are entangled with each other and can be individually manipulated and detected to demonstrate quantum gain in joint multiparameter estimation of a set of parameters imprinted on the array and their nonlocal linear combinations. Our experiment shows that intersensor entanglement enhances the performance of sensor arrays (*18*, *29*) and constitutes a notable proof of concept for quantum-enhanced field sensors and imaging devices (*27*).

Joint multiparameter estimation

Consider an array of M quantum sensors operating in parallel (*18*, *27*, *29*), each consisting of an ensemble of N_k two-level atoms that form a collective spin (*5*) $\mathbf{S}_k$, with $k = 1,\ldots,M$ (Fig. 1). Each sensor is located at a distinct spatial position $\mathbf{r}_k$ and measures the local value of an external field $B(\mathbf{r}_k)$, which is imprinted as a rotation of angle $\theta_k \propto B(\mathbf{r}_k)$ onto the sensor spin. The collection of parameters $\boldsymbol{\theta} = (\theta_1,\ldots,\theta_M)$ thus provides discrete sampling of the spatial distribution of $B(\mathbf{r})$, enabling reconstruction of the field profile. Here, B is a magnetic field, but other quantities such as electric fields or gravity can be imprinted in a similar way through evolution with suitable Hamiltonians.

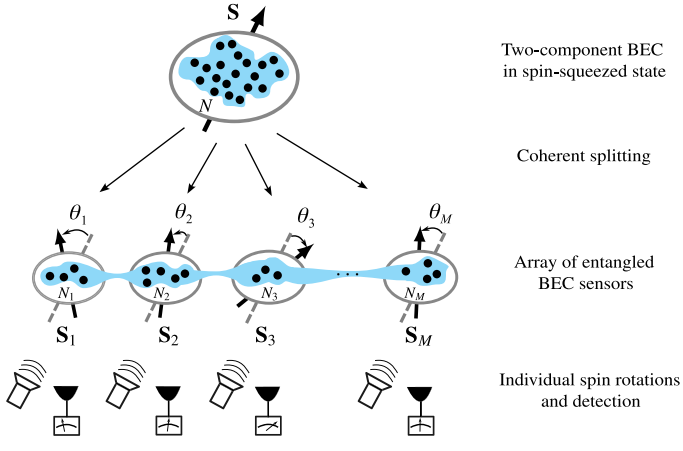

Fig. 1. Array of entangled atomic sensors for multiparameter estimation. An array of M sensors, each consisting of a collective spin $\mathbf{S}_k$ of N_k two-level atoms, is used to determine M parameters $\theta_1, \theta_2,\ldots,\theta_M$ that are encoded on the sensors as local spin rotations. The sensor spins are prepared by coherently splitting a two-component BEC in a spin-squeezed state, resulting in entanglement between atoms within each sensor and between different sensors. In combination with individual spin rotations and detection, the entanglement enables a statistical gain in the determination of the M parameters compared with the case without quantum correlations.

The sensors are read out by measuring suitable components of each $\mathbf{S}_k$, and the whole experiment is repeated μ times. The goal of multiparameter quantum metrology is to jointly estimate with the highest possible precision the local parameters θ_k or certain nonlocal combinations $\mathbf{n}\cdot\boldsymbol{\theta} = n_1\theta_1 + \ \ldots\ + n_M\theta_M$, where $\mathbf{n} = (n_1,\ldots,n_M)$ is a unit vector of coefficients determining the specific linear combination of interest. For example, in the case of $M = 2$ ensembles, $\mathbf{n}_+ = (1,1)/\sqrt{2}$ gives a measurement of the sum $\theta_+ = (\theta_1+\theta_2)/\sqrt{2}$ and $\mathbf{n}_- = (1,-1)/\sqrt{2}$ a measurement of the difference $\theta_- = (\theta_1-\theta_2)/\sqrt{2}$ of the parameters, corresponding to the average field and the field gradient, respectively.

In such a multiparameter estimation task, the optimal management of resources is a complex problem (*18*, *20*, *21*, *22*, *28*, *29*, *30*), and the expected performance depends on the scenario considered. In accordance with the experimental constraints and capabilities, we consider the total number of atoms $N = \sum_{k=1}^{M} N_k$ and the total number of preparations μ of the system as fixed resources and assume that every sensor can be manipulated and measured individually. The performance of such a sensor array has been theoretically analyzed (*18*, *29*), showing that entanglement between the atoms in each ensemble as well as entanglement between the different ensembles can enhance the measurement precision compared with the case of nonentangled atoms. Moreover, it has been shown that entanglement both within and between the ensembles is necessary to achieve the highest performance in estimating a single nonlocal parameter combination (*18*).

Multiparameter squeezing (*29*), also called multimode squeezing in other contexts (*40*), is a particularly promising strategy for quantum enhancement in sensor arrays. Similar to spin-squeezing of a single atomic ensemble (*45*, *46*), which has been the most successful approach to quantum metrology with atomic sensors (*5*), it is comparatively simple to generate, compatible with standard interferometric sequences and detection methods, and robust against decoherence. A multiparameter squeezed state features quantum correlations of the sensor spins $\mathbf{S}_k$ that squeeze the noise in the measurement of specific combinations of the parameters θ_k. For nonlocal parameter combinations, this requires nonlocal squeezing in a corresponding superposition of sensor modes. For example, if the whole sensor array is prepared in a squeezed state of the global spin $S = \sum_{k=1}^{M} \mathbf{S}_k$ and the atoms are equally distributed, that is $N_k = N/M$, the linear combination corresponding to the sum $(\theta_1 + \ \ldots\ + \theta_M)/\sqrt{M}$ of all parameters can be measured with quantum gain, whereas all other orthogonal combinations will be measured with a statistical uncertainty greater than that for independent atoms [see (*47*), section 3.1]. However, as we show theoretically and experimentally, local rotations of the individual sensor spins $\mathbf{S}_k$ can reconfigure the quantum correlations between the sensors, allowing us to achieve quantum enhancement for multiple parameters jointly, using global squeezing of the initial state as the resource (*27*). Moreover, a suitable distribution N_k of atoms into the M sensors in combination with local rotations allows us to enhance the measurement of any parameter combination $\mathbf{n}\cdot\boldsymbol{\theta}$ of interest (*27*, *29*, *47*).

Preparation of entangled sensor array

In our experiment, the atomic sensor array was realized by spatially splitting a spin-squeezed BEC of $N \approx 1450$ ^{87}Rb atoms (*10*) into the M ensembles using coherent splitting techniques similar to those in (*48*), which we extended here to enable splitting into more than two ensembles and to adjust the splitting ratios as desired while maintaining full coherent control (*47*).

In each ensemble k, the atoms were prepared in a superposition of hyperfine ground states $|k\uparrow\rangle$ and $|k\downarrow\rangle$ that define the collective spin (*5*) $\mathbf{S}_k$. Arbitrary spin rotations could be applied to each sensor individually by coupling the states with resonant microwave and radio frequency magnetic fields. By absorption detection of the atom numbers $N_{k\uparrow}$ and $N_{k\downarrow}$ in the two states, we could directly measure $N_k = N_{k\uparrow} + N_{k\downarrow}$ and the collective spin component $S_k^z = (N_{k\uparrow} - N_{k\downarrow})/2$.

As a source of entanglement, we prepared the initial BEC in a spin-squeezed state of the global spin $\mathbf{S}$, where all atomic spins are entangled with each other (*5*). Using controlled atomic collisions on an atom chip (*10*), we prepared states with a Wineland spin-squeezing parameter $\xi^2 = N\mathrm{Var}(S_z)/|\langle S_x\rangle|^2 \approx -6.5(2)$ dB and spin length $\langle S_x\rangle = CN/2$ with contrast $C = 0.94(1)$. Upon spatial splitting into the sensor clouds (*47*), the spin-squeezing results in Einstein-Podolsky-Rosen entanglement between the sensor spins $\mathbf{S}_k$, as illustrated in Fig. 1 and as we have demonstrated previously for two clouds (*48*). In this work, we extended this technique to multiple ensembles and used it as a resource for multiparameter quantum metrology.

Joint estimation with two entangled sensors

We first demonstrated joint multiparameter estimation with two entangled atomic sensors (Fig. 2). The ensemble was symmetrically split,

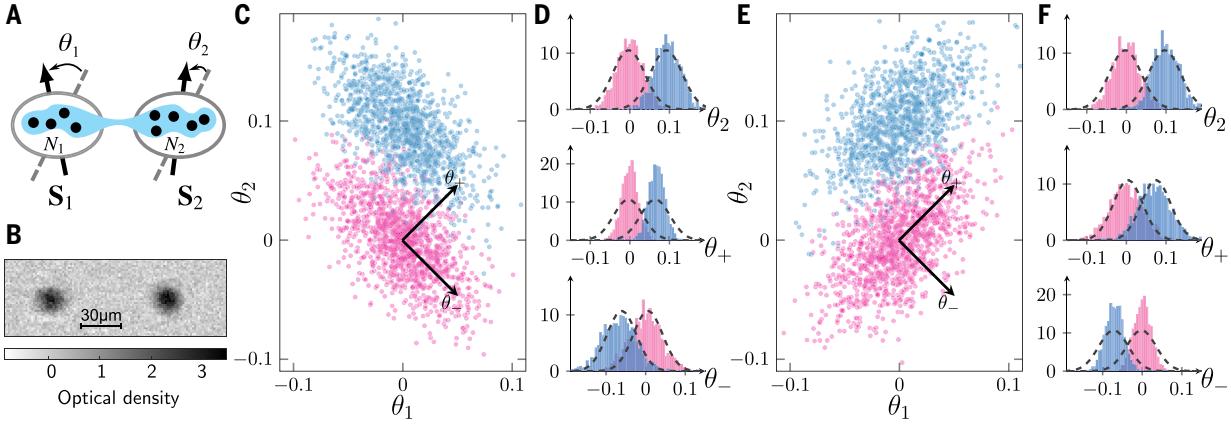

Fig. 2. Joint estimation of two parameters with two entangled atomic sensors. (**A**) Parameters θ_1 and θ_2 are imprinted on the two sensor spins. (**B**) Absorption image of the two atomic clouds with $N_1 \approx N_2$. (**C**) Correlation plot of simultaneous measurements of θ_1 and θ_2 showing strong correlations owing to the intersensor entanglement. Two datasets are shown for two different values of θ_2, each with 1200 repetitions (purple and blue, respectively). (**D**) Histograms obtained from the measurements in (C) for θ_2 (top), θ_+ (middle), and θ_- (bottom). The measurement of θ_+ exploits the intersensor entanglement, resulting in the smallest variances. Dashed lines represent the distribution for an ideal coherent spin state. (**E**) Correlation plot similar to (C) but for measurements with a π pulse applied to $\mathbf{S}_2$ prior to parameter imprinting. (**F**) Histograms for the data in (E). Now, the measurement of θ_- shows minimal variance owing to the entanglement.

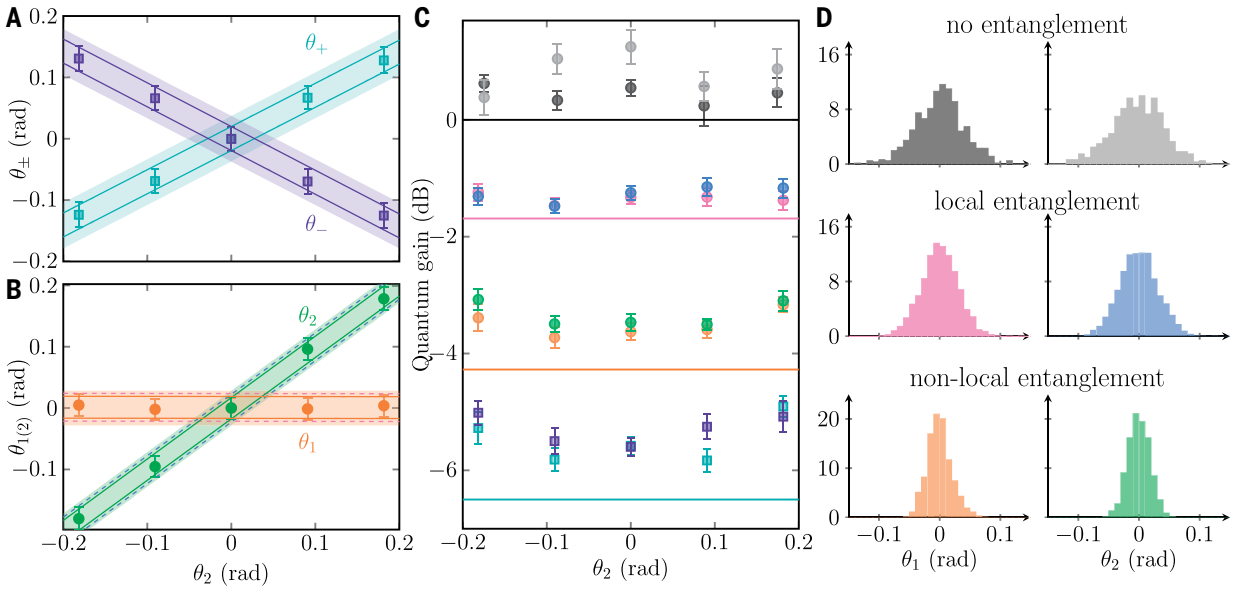

Fig. 3. Joint estimation of two local parameters enhanced by nonlocal squeezing. (**A**) Measurement results of θ_+ (teal) and θ_- (violet) for different applied rotations θ_2. Error bars, standard deviation (SD) of measurement outcomes; solid lines, linear fit to SD; shaded areas, SQL for an ideal coherent spin state. (**B**) Joint estimation of θ_1 (orange) and θ_2 (green) from properly weighted measurements of θ_+ and θ_-, as described in the text, with error bars and solid lines indicating SD as in (A). Dashed lines, SD obtained if intersensor entanglement is ignored; shaded areas, SQL. (**C**) Comparison of quantum gains for estimating θ_1 and θ_2 using different strategies: Unentangled atoms (gray and light gray), local measurements ignoring intersensor entanglement (pink and blue), and joint estimation using nonlocal entanglement (orange and green). Solid lines indicate the corresponding theoretical expectations. The square points in teal and violet show the quantum gain for estimating only θ_+ or only θ_-, respectively. The teal line represents initial squeezing. All error bars represent standard errors of the mean. (**D**) Histograms of the measurements of θ_1 and θ_2 at an applied $\theta_2 = 0$ using the same colors as in (C). The top histograms show results for unentangled atoms. The histograms in the middle and bottom rows show data from the same experimental runs with entangled atoms. In the middle row, local estimators only make use of local entanglement within each sensor. In the bottom row, joint estimation also makes use of the nonlocal entanglement between the sensors.

$N_1 \approx N_2 \approx N/2$, and the sensor spins were initially polarized along S_k^x. The parameters θ_1 and θ_2 were encoded as small angle rotations of the two sensor spins around the y axis. By measuring the atom numbers in all four states involved, the parameters could be directly estimated as $\theta_k \approx S_k^z / \langle S_k^x \rangle = (N_{k\uparrow} - N_{k\downarrow}) / C_k \langle N_k \rangle$. Figure 2C shows such simultaneous measurements of θ_1 and θ_2, one dataset with and one without a shift applied to θ_2. Local entanglement in each ensemble reduces the variance of both θ_1 and θ_2 by −1.3(2) dB below the SQL, as can be seen in the top histograms in Fig. 2D and in Fig. 3C (pink and blue points). However, such an estimation strategy does not exploit the entanglement between the sensors, which manifests itself in strong correlations between the measurement outcomes of θ_1 and θ_2.

To exploit the intersensor entanglement, we estimated the nonlocal parameter $\theta_+ = (\theta_1 + \theta_2)/\sqrt{2}$, which is sensitive to the squeezed global spin component $S^z = S_1^z + S_2^z$ and can be estimated with a variance of $\mathrm{Var}(\theta_+) = 2\xi^2/\mu N$ using N atoms and μ repetitions of the experiment [see (*47*), section 3]. Compared with the SQL obtained with unentangled atoms in an ideal coherent spin state, $\mathrm{Var}_{\mathrm{SQL}}(\theta_\pm) = 2/\mu N$, the full enhancement ξ^2 provided by the spin-squeezed state can be recovered in this way. For the data in Fig. 2C, we found that $\mathrm{Var}(\theta_+)$ was reduced by −5.6(2) dB below the SQL, which is evident in the narrow histogram in Fig. 2D and quantitatively shown in Fig. 3C (teal square points). The orthogonal linear combination $\theta_- = (\theta_1 - \theta_2)/\sqrt{2}$, on the other hand, which we can also access owing to the individual readout of the sensors, was estimated from the same data with a variance $\mathrm{Var}(\theta_-) \approx 2/\mu NC^2$, slightly above the SQL.

Alternatively, we can apply a local π rotation to invert the sign of S_2^z prior to imprinting the parameters. This transfers the quantum correlations between the sensors into the antisymmetric mode so that $S_1^z - S_2^z$ is squeezed. Now, θ_- can be estimated with $\mathrm{Var}(\theta_-) = 2\xi^2/\mu N$, whereas $\mathrm{Var}(\theta_+) \approx 2/\mu NC^2$ remains above the SQL. Figure 2, E and F, show data taken in this way. From these measurements, we obtained an improvement of −5.6(2) dB below the SQL in $\mathrm{Var}(\theta_-)$, as shown in Fig. 3C (violet square points).

Our strategy to estimate both θ_+ and θ_- with quantum enhancement was to alternate between these two settings, performing $\mu/2$ measurements with and $\mu/2$ without the π rotation of $\mathbf{S}_2$, respectively, so that the overall resources are unchanged. To fully exploit the information provided by both sets of measurements, we estimated both θ_+ and θ_- in each of the two settings, resulting in four estimates that we combined with appropriate statistical weights, as discussed in (*47*), section 3.2. This allowed us to jointly estimate θ_+ and θ_-, theoretically with identical uncertainties $\mathrm{Var}(\theta_\pm) = \frac{4}{\mu N}\frac{\xi^2}{1+C^2\xi^2}$. With respect to the SQL, the gain here is $\frac{2\xi^2}{1+C^2\xi^2} \approx 2\xi^2$ for $\xi^2 \ll 1$. Because the estimators for (θ_1, θ_2) are orthonormal linear combinations of (θ_+, θ_-), they can be obtained with the same variances $\mathrm{Var}(\theta_{1,2}) = \mathrm{Var}(\theta_\pm)$ from the same dataset. Figure 3 shows experimental data for such joint estimation of the local parameters θ_1 and θ_2, using the nonlocal squeezed state as a resource for quantum enhancement. The observed improvement beyond the SQL was −3.6(2) dB for θ_1 and −3.5(1) dB for θ_2 (Fig. 3C). Theoretically, we expected −4.3(2) dB given the initial squeezing of $\xi^2 = -6.5(2)$ dB and a contrast of $C = 0.94(1)$, in good agreement with the experiment, given that we did not subtract any technical noise (*47*).

The variances $\mathrm{Var}(\theta_{1,2})$ that we obtained with our protocol equal the harmonic average $\overline{\sigma}^H$ of the eigenvalues of the covariance matrix $\mathrm{Cov}(\theta_k, \theta_l)$ of the local estimators $\theta_k = S_k^z / \langle S_k^x \rangle$ in the initial, symmetrically split, spin-squeezed state. The harmonic average is smaller than or equal to the arithmetic average corresponding to the trace of the covariance matrix, and we identified it here as the relevant figure of merit [see (*47*), sections 3.2 and 3.3].

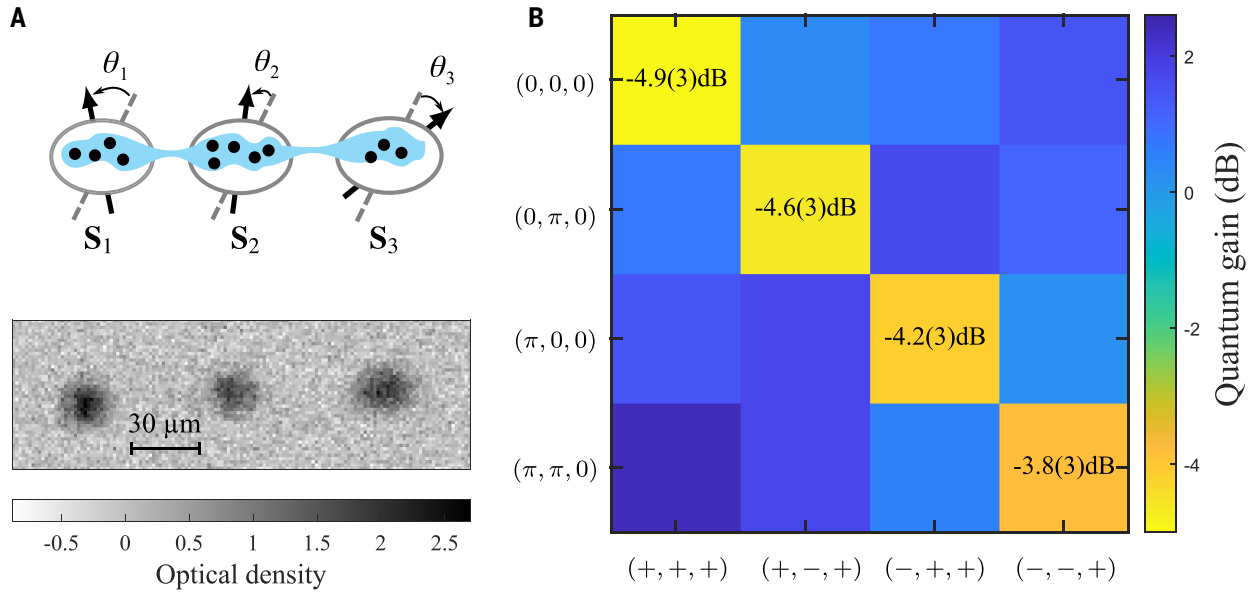

Fig. 4. Joint multiparameter estimation with $M = 3$ entangled atomic sensors. (**A**) Schematic of the three entangled sensor spins on which three local parameters are imprinted (top) and an absorption image of the three atomic clouds (bottom). (**B**) Matrix of metrological gains compared with the SQL for four different sensor preparations and four estimated parameter combinations. Each row corresponds to a different preparation with π pulses applied to the spins ($\mathbf{S}_1$, $\mathbf{S}_2$, $\mathbf{S}_3$), as indicated. Each colum corresponds to the estimation of a different linear combination $(\pm 0.644\,\theta_1 \pm 0.431\,\theta_2 + 0.632\,\theta_3)$ with signs (±, ±, +), as indicated. Quantum gain is observed on the diagonal, where the sensor configuration matches the parameter combination.

For an ideal spin-squeezed state with a large number of atoms, it can be further shown that $\overline{\sigma}^H$ reaches the harmonic average is the eigenvalues of $(\mu F)^{-1}$, where μ is the number of system preparations, and F is the multiparameter quantum Fisher information matrix. This shows that this strategy, which is demonstrated in this work experimentally, is the optimal strategy for the resources at hand (a spin-squeezed state split symmetrically between the sensors) in that it saturates the corresponding Cramer-Rao bound [see (*47*), section 3.3].

In certain measurement tasks, only a single linear combination of local parameters $\mathbf{n} \cdot \boldsymbol{\theta}$ is of interest, such as in field gradiometry or, more generally, in measuring a particular multipole moment or Fourier component of a field with a sensor array. In this case, the optimal measurement configuration requires a specific distribution of resources to the sensors (*49*), which, in our case, amounts to a particular distribution of local atom numbers N_k (*47*). We experimentally demonstrated this for the case of two sensors and different distributions of atoms. In the ideal case, this strategy allows exploitation of the full enhancement ξ^2 provided by the initial spin-squeezed state. In the experiment, we obtained about −5.5-dB enhancement for all investigated nonlocal parameter combinations (fig. S2).

More than two entangled sensors

We extended our multiparameter metrology scheme to larger sensor arrays, which raised fresh conceptual questions on the optimal use of the entanglement in the nonlocal squeezed state. For M sensors containing $N_k = N/M$ atoms each, estimating the parameters (θ_1, θ_2,...,θ_M) with a globally squeezed state, the question arose as to what sensor configurations should be prepared, i.e., which of the sensor spins should be subject to π rotations prior to parameter imprinting. We can show that the estimation strategy based on the Hadamard matrix of order M, whose elements ±1 define which sensor spins should be rotated, is optimal (*27*), as discussed in (*47*), section 3.3. However, Hadamard matrices can only exist for dimensions one, two, and multiples of four. For other dimensions, we must resort to a truncated version of the next-higher Hadamard matrix, whose rows define the sensor configurations. The simplest case that demonstrates this concept is $M = 3$, where four different configurations of the sensor array have to be prepared to jointly estimate the three local parameters (θ_1, θ_2, θ_3) in an optimal way, corresponding to the rows of a Hadamard matrix of order four with one column truncated. The theoretically expected uncertainty is $\mathrm{Var}(\theta_k) = \frac{M}{\mu N} \cdot \frac{M\xi^2}{1+(M-1)C^2\xi^2}$ where the first factor is the SQL, and the second factor the quantum gain, as discussed in (*47*), section 3.4.

In Fig. 4, we present data demonstrating joint multiparameter estimation with $M = 3$ entangled atomic sensors. We split the spin-squeezed BEC into three clouds with $N_1 = 630(30)$, $N_2 = 420(20)$, and $N_3 = 620(30)$, retaining −4.9(3) dB of squeezing in the global spin $S^z = S_1^z + S_2^z + S_3^z$ after splitting (*47*). We prepared four different sensor configurations by applying local π rotations to the $\mathbf{S}_k$, as indicated in Fig. 4B. For each configuration, we observed a quantum gain of around −4 dB beyond the SQL for the linear combination of parameters that matched the sensor configuration. For this dataset, these combinations were $(\pm 0.644\,\theta_1 \pm 0.431\,\theta_2 + 0.632\,\theta_3)$ because of the imbalance in N_k (*47*). Combining the data from all four settings, we could jointly estimate all three local parameters $(\theta_1, \theta_2, \theta_3)$ with quantum gains of [−1.7(2), −0.8(2), −1.8(2)] dB beyond the SQL for the same overall resources N and μ. If we omitted any of the four prepared sensor configurations in the analysis, then we obtained lower quantum gains in all three parameters for the same overall N and μ, confirming the quantum advantage of four sensor configurations over three in the case $M = 3$.

Discussion and outlook

In this work, we have experimentally demonstrated quantum-enhanced multiparameter sensing with arrays of up to three atomic sensors. The theoretical analysis shows that our estimation protocol can be extended to an arbitrary number of entangled sensors. Although the protocol is optimal for our resources, as the number M of jointly estimated parameters increases, the quantum gain for each parameter decreases with M, reflecting the fact that only a single collective mode

of the array is squeezed in each experimental run but used to enhance all M parameters.

An intriguing perspective for multiparameter estimation with larger sensor arrays is compressed sensing (*27*), also called multiparameter estimation with nuisance parameters (*50*, *51*), where one is only interested in a subset L_H of all possible nonlocal parameter combinations, with $L_H \ll M \ll N$. By specifically preparing sensor configurations that enhance the L_H linear combinations of interest, substantial quantum gains can be achieved, which is particularly relevant for field imaging and pattern recognition applications (*27*).

Our experiment demonstrates multiparameter estimation using globally squeezed states. This technique could be transferred to state-of-the-art atomic precision sensors, such as optical lattice clocks (*16*), where entanglement between subensembles in different lattice sites could improve the measurement of gravitational redshifts at short length scales or the characterization of spatially dependent systematic effects. More generally, our results lay the groundwork for future demonstrations of intriguing sensing schemes, such as the entanglement of distant atomic clocks (*52*), opening up possibilities to study gravitational decoherence (*53*) and long baseline gravitational wave detection using atom interferometry (*54*). Furthermore, our experimental system with collective spins of spatially separated atomic ensembles entangled by one-axis twisting evolution is also well-suited for the realization of recent proposals for vector magnetometry (*24*), which involve simultaneous sensing of orthogonal magnetic field components for which the Hamiltonians do not commute and the optimal measurements are incompatible.

REFERENCES AND NOTES

1. A. D. Ludlow, M. M. Boyd, J. Ye, E. Peik, P. O. Schmidt, *Rev. Mod. Phys.* **87**, 637–701 (2015).
2. D. Budker, M. Romalis, *Nat. Phys.* **3**, 227–234 (2007).
3. A. D. Cronin, J. Schmiedmayer, D. E. Pritchard, *Rev. Mod. Phys.* **81**, 1051–1129 (2009).
4. V. Giovannetti, S. Lloyd, L. Maccone, *Science* **306**, 1330–1336 (2004).
5. L. Pezzè, A. Smerzi, M. K. Oberthaler, R. Schmied, P. Treutlein, *Rev. Mod. Phys.* **90**, 035005 (2018).
6. A. Sinatra, *Appl. Phys. Lett.* **120**, 120501 (2022).
7. J. Estève, C. Gross, A. Weller, S. Giovanazzi, M. K. Oberthaler, *Nature* **455**, 1216–1219 (2008).
8. J. Appel *et al.*, *Proc. Natl. Acad. Sci. U.S.A.* **106**, 10960–10965 (2009).
9. M. H. Schleier-Smith, I. D. Leroux, V. Vuletić, *Phys. Rev. Lett.* **104**, 073604 (2010).
10. M. F. Riedel *et al.*, *Nature* **464**, 1170–1173 (2010).
11. C. Gross, T. Zibold, E. Nicklas, J. Estève, M. K. Oberthaler, *Nature* **464**, 1165–1169 (2010).
12. I. D. Leroux, M. H. Schleier-Smith, V. Vuletić, *Phys. Rev. Lett.* **104**, 073602 (2010).
13. R. J. Sewell *et al.*, *Phys. Rev. Lett.* **109**, 253605 (2012).
14. W. J. Eckner *et al.*, *Nature* **621**, 734–739 (2023).
15. M.-Z. Huang *et al.*, *PRX Quantum* **4**, 020322 (2023).
16. J. M. Robinson *et al.*, *Nat. Phys.* **20**, 208–213 (2024).
17. T. B. Magdalena Szczykulska, A. Datta, *Adv. Phys. X* **1**, 621–639 (2016).
18. M. Gessner, L. Pezzè, A. Smerzi, *Phys. Rev. Lett.* **121**, 130503 (2018).
19. R. Demkowicz-Dobrzański, W. Górecki, M. Guţă, *J. Phys. A Math. Theor.* **53**, 363001 (2020).
20. J. Liu, H. Yuan, X.-M. Lu, X. Wang, *J. Phys. A Math. Theor.* **53**, 023001 (2020).
21. J. S. Sidhu, P. Kok, *AVS Quantum Sci.* **2**, 014701 (2020).
22. F. Albarelli, M. Barbieri, M. Genoni, I. Gianani, *Phys. Lett. A* **384**, 126311 (2020).
23. L. Pezzè, A. Smerzi, arXiv:2502.17396 [quant-ph] (2025).
24. R. Kaubruegger, A. Shankar, D. V. Vasilyev, P. Zoller, *PRX Quantum* **4**, 020333 (2023).
25. X. Meng *et al.*, *Nat. Commun.* **14**, 6105 (2023).
26. J. Řehaček *et al.*, *Phys. Rev. A* **96**, 062107 (2017).
27. Y. Baamara, M. Gessner, A. Sinatra, *SciPost Phys.* **14**, 050 (2023).
28. T. J. Proctor, P. A. Knott, J. A. Dunningham, *Phys. Rev. Lett.* **120**, 080501 (2018).
29. M. Gessner, A. Smerzi, L. Pezzè, *Nat. Commun.* **11**, 3817 (2020).
30. W. Górecki, R. Demkowicz-Dobrzański, *Phys. Rev. A* **106**, 012424 (2022).
31. R. Corgier, M. Malitesta, A. Smerzi, L. Pezzè, *Quantum (Vienna)* **7**, 965 (2023).
32. M. Malitesta, A. Smerzi, L. Pezzè, *Phys. Rev. A* **108**, 032621 (2023).
33. M. Fadel, B. Yadin, Y. Mao, T. Byrnes, M. Gessner, *New J. Phys.* **25**, 073006 (2023).
34. P. Kómár *et al.*, *Nat. Phys.* **10**, 582–587 (2014).
35. S. Ragy, M. Jarzyna, R. Demkowicz-Dobrzański, *Phys. Rev. A* **94**, 052108 (2016).
36. A. Carollo, B. Spagnolo, A. A. Dubkov, D. Valenti, *J. Stat. Mech.* **2019**, 094010 (2019).
37. A. Z. Goldberg, A. B. Klimov, G. Leuchs, L. L. Sánchez-Soto, *JPhys Photonics* **3**, 022008 (2021).
38. A. Hamann, P. Sekatski, W. Dür, *Quantum Sci. Technol.* **9**, 035005 (2024).
39. G. Colangelo, F. M. Ciurana, L. C. Bianchet, R. J. Sewell, M. W. Mitchell, *Nature* **543**, 525–528 (2017).
40. X. Guo *et al.*, *Nat. Phys.* **16**, 281–284 (2020).
41. B. K. Malia, Y. Wu, J. Martínez-Rincón, M. A. Kasevich, *Nature* **612**, 661–665 (2022).
42. M. Lipka, A. Sierant, C. Troullinou, M. W. Mitchell, *Phys. Rev. Appl.* **21**, 034054 (2024).
43. W. Muessel, H. Strobel, D. Linnemann, D. B. Hume, M. K. Oberthaler, *Phys. Rev. Lett.* **113**, 103004 (2014).
44. D. Schäffner, T. Schreiber, F. Lenz, M. Schlosser, G. Birkl, *PRX Quantum* **5**, 010311 (2024).
45. M. Kitagawa, M. Ueda, *Phys. Rev. A* **47**, 5138–5143 (1993).
46. D. J. Wineland, J. J. Bollinger, W. M. Itano, F. L. Moore, D. J. Heinzen, *Phys. Rev. A* **46**, R6797–R6800 (1992).
47. See supplementary materials.
48. P. Colciaghi, Y. Li, P. Treutlein, T. Zibold, *Phys. Rev. X* **13**, 021031 (2023).
49. L. Pezzè, A. Smerzi, arXiv:2405.18404 [quant-ph] (2024).
50. J. Suzuki, Y. Yang, M. Hayashi, *J. Phys. A Math. Theor.* **53**, 453001 (2020).
51. J. A. Gross, C. M. Caves, *J. Phys. A Math. Theor.* **54**, 014001 (2020).
52. E. S. Polzik, J. Ye, *Phys. Rev. A* **93**, 021404 (2016).
53. I. Pikovski, M. Zych, F. Costa, Č. Brukner, *Nat. Phys.* **11**, 668–672 (2015).
54. J. M. Hogan, M. A. Kasevich, *Phys. Rev. A* **94**, 033632 (2016).
55. Y. Li, L. Joosten, P. Colciaghi, P. Treutlein, T. Zibold, Quantum enhanced multiparameter sensing data, Zenodo (2025); https://doi.org/10.5281/zenodo.17176452.

ACKNOWLEDGMENTS

The authors thank Y. Castin, R. Demkowicz-Dobrzański, A. Hamann, L. Pezzè, and P. Sekatski for helpful discussions. **Funding:** The experiments in Basel were supported by the Swiss National Science Foundation. Y.B. thanks Quantum Information Center Sorbonne for financial support. **Author contributions:** A.S. and P.T. initiated the study. Y.L., L.J., P.C., and T.Z. improved the experimental apparatus. Y.L., L.J., and P.C. performed experiments and analyzed the data under the supervision of T.Z. and P.T.. Y.B. and A.S. peformed the theoretical analysis, discussing with the other authors. All authors discussed the results and contributed to the manuscript. **Competing interests:** The authors declare that they have no competing interests. **Data, code, and materials availability:** The study involved no new materials preparation. All data needed to evaluate the conclusions in the paper are present in the figures of the paper. The data can be accessed at Zenodo (*55*).

SUPPLEMENTARY MATERIALS

science.org/doi/10.1126/science.adt2442
Materials and Methods; Supplementary Text; Figs. S1 and S2; References (*56-60*)

Submitted 18 September 2024; accepted 20 November 2025

10.1126/science.adt2442